

Article

Sensor Incipient Fault Impacts on Building Energy Performance: A Case Study on a Multi-Zone Commercial Building

Yanfei Li ¹, Piljae Im ^{2,*}, Seungjae Lee ³, Yeonjin Bae ¹, Yeobeom Yoon ² and Sangkeun Lee ⁴

¹ Electrification and Energy Infrastructures Division, Building Technologies Research and Integration Center, Oak Ridge National Laboratory, 1 Bethel Valley Rd, Oak Ridge, TN 37830, USA

² Buildings and Transportation Science Division, Building Technologies Research and Integration Center, Oak Ridge National Laboratory, 1 Bethel Valley Rd, Oak Ridge, TN 37830, USA

³ Department of Civil and Mineral Engineering, University of Toronto, 35 St. George St, Toronto, ON M5S 1A4, Canada

⁴ Computer Science and Mathematics Division, Oak Ridge National Laboratory, 1 Bethel Valley Rd, Oak Ridge, TN 37830, USA

* Correspondence: imp1@ornl.gov

Abstract: Existing studies show sensor faults/error could double building energy consumption and carbon emissions compared with the baseline. Those studies assume that the sensor error is fixed or constant. However, sensor faults are incipient in real conditions and there were extremely limited studies investigating the incipient sensor fault impacts systematically. This study filled in this research gap by studying time-developing sensor fault impacts to rule-based controls on a 10-zone office building. The control sequences for variable air volume boxes (VAV) with an air handling unit (AHU) system were selected based on ASHRAE Guideline 36-2018: High-Performance Sequences of Operation for HVAC Systems. Large-scale simulations on cloud were conducted (3600 cases) through stochastic approach. Results show (1) The site energy differences could go −3.3% lower or 18.1% higher, compared with baseline. (2) The heating energy differences could go −66.5% lower or 314.4% higher, compared with baseline. (3) The cooling energy differences could go −11.5% lower or 65.0% higher, compared with baseline. (4) The fan energy differences could go 0.15% lower or 6.9% higher, compared with baseline.

Keywords: building energy; sensor impact; building control; incipient sensor faults



Citation: Li, Y.; Im, P.; Lee, S.; Bae, Y.; Yoon, Y.; Lee, S. Sensor Incipient Fault Impacts on Building Energy Performance: A Case Study on a Multi-Zone Commercial Building. *Buildings* **2023**, *13*, 520. <https://doi.org/10.3390/buildings13020520>

Academic Editors: Rafik Belarbi and Md Morshed Alam

Received: 13 December 2022

Revised: 19 January 2023

Accepted: 7 February 2023

Published: 14 February 2023



Copyright: © 2023 by the authors. Licensee MDPI, Basel, Switzerland. This article is an open access article distributed under the terms and conditions of the Creative Commons Attribution (CC BY) license (<https://creativecommons.org/licenses/by/4.0/>).

1. Introduction

The building sector consumes 40% of energy consumption and 16% carbon emissions in the United States, based on the 2020 Energy Outlook from the United States Energy Information Administration [1]. It has remained a challenge to reduce building energy consumption and carbon emissions, although many advanced building technologies have been proposed. A few well-known technologies are continually evolving, such as ground source heat pumps [2] and heat pumps in cold climates [3], with the goal of building electrifications and carbon reductions. For any of those building heating/cooling equipment, control loops are an essential part of the system, aiming for optimal operation to reduce energy consumption, power demands, and carbon emissions.

In the past 10 years, building controls have been actively advancing and sensors have not been well studied. Sensors are critical components for controls systems, collecting inputs to controls for subsequent control actions. When sensors work in fault (or unhealthy) conditions, the control benefits will be compromised regardless of the effectiveness of the controls [4]. Buildings are easily operating under fault conditions [5]. For buildings, multiple components directly influence the sensor placement and deployment, such as sensor errors, sensor locations, sensor types, and sensor costs [4].

Sensors are usually calibrated by manufacturers. However, sensor accuracy might drift with time after being installed. There are many reasons for sensor abnormalities, such as harsh environments and manufacturing defects. In such scenarios, sensor reading accuracy might suffer, which is commonly regarded as a sensor fault. Usually, HVAC systems have multiple sensors to assist the controls and multiple sensors might have multiple faults [6]. A study described a total of nine types of sensor fault patterns based on measurement datasets [7]:

- **Outlier:** usually a small number of isolated sensor readings, unexpectedly far from the majority of normal readings. This reason is usually unknown but could be related to the data logger;
- **Spike:** a pattern with a much higher rate of change for multiple data points or sensor readings in a short time period. It might be related to battery failure, other hardware failure, or connection issues;
- **Stuck-at:** a pattern with zero variance or constant sensor readings or data points. The reason is usually associated with hardware malfunction;
- **High noise or variance:** a pattern with higher variance or noise than historical data suggests or normally expects for sensor readings or data points. The reasons might be associated with hardware failure, environmental conditions, or weakening battery power;
- **Calibration:** a pattern in which the sensor readings are always offset from ground truth values. It might be related to calibration error or sensor drifting. Often, incipient sensor drift (the amount of drift change with time) is also common in modern sensors;
- **Connection or hardware:** usually inaccurate sensor readings because of malfunctioning hardware (i.e., hardware dependent). Typical patterns are unusually high/low data readings that are frequently out of normal ranges. The possible reasons might be environment changes, sensor aging, short circuit, or loose wires;
- **Low battery:** usually inaccurate sensor readings because of low battery power. Typical patterns are unexpected gradient followed by zero variance, or lack of data, or excessive noise;
- **Environment out of range:** when the environment conditions go beyond what the sensor system can read. Typical examples are extreme high and low temperatures. Patterns might be much higher noise or flattening of the data. Similar patterns occur with improper calibrations;
- **Clipping:** sensor readings max out. The patterns could be sticking with maximum or minimum readings, perhaps because of environmental conditions.

Multiple sensors (e.g., temperature, flowrate) usually work together as a sensor sets. Sensor sets are different, depending on the HVAC system types and the controls loops. HVAC systems vary based on different building characteristics and functions. For small to medium office buildings, rooftop units (RTUs) are usually used. Typical sensors are air-related [8], such as air temperature, airflow rate, and pressure sensors. For large commercial buildings (e.g., large office buildings), a chiller and cooling tower are usually applied. More sensors are placed on water loops [9], such as water flow rate and water temperature sensors. There are three types of controls: rule-based control, local control, and supervisory control for HVAC systems. Different control strategies might require different sensor sets. Demand control ventilations need zone CO₂ sensors for control actions [8,10]. Occupant control, relying on occupant sensors, is another popular topic attracting attention in the past few years [11,12].

In the context of buildings and HVAC systems, limited studies have investigated sensor fault impacts on HVAC systems. Past studies show that the impact of sensor faults poses a great challenge to optimal performance of advanced control solutions [13,14]. Sensor fault modeling study could be classified into two groups: white-box and black-box [5,15]. The majority of studies applied the white-box method. Black-box method is suitable for fault detection. Due to the severe fault impacts, sensor calibration and fault mitigation become more important. The detailed literature reviews are summarized as:

- (1) A study investigated sensor impact on building energy consumption [16], through a small office model in the EnergyPlus platform. Their study proposed a new concept for sensor fault impacts: one-way impact and two-way impact. The one-way impact means that sensor faults cause decreased or increased energy consumption or thermal comfort. The two-way impact means that there could be higher energy consumption for a certain desired energy item (e.g., cooling), and simultaneously lower energy consumption for another desired energy item (e.g., heating). Another recent study proposed the sensor fault impact analysis framework [9] to investigate sensor fault impacts. This framework is based on white-box methods, which opened a door for sensor fault studies on building performance. Their results show that sensors could cause more than double energy consumption. Another study, using white-box modeling platform, demonstrated sensor fault impacts for demand control ventilation (DCV) on building energy consumption [8]. Results show that sensor faults severely downgraded the control performance, leading to increased energy consumption. Another recent study developed a few fault models in the EnergyPlus platform, which were validated through experiments [17,18];
- (2) Black-box, or machine learning algorithm, is becoming a new trend in fault detection and diagnostics. This study applied artificial intelligence (AI) algorithms to detect the sensor faults, based on a large dataset. A review study [19] pointed out the biggest issue for black-box method is how to identify the baseline data (data without fault) from the building energy management system;
- (3) Sensor fault calibration and mitigation are receiving attention. This study aimed to calibrate the sensor faults [20], to which they applied the virtual in-situ calibration method. Their results showed that the systematic errors of sensors were less than 2% and the random errors were also reduced by as much as 74%. The benefit of such sensor calibration significantly reduced the possibility of abnormal data and enhanced the reliability of sensor measurements. This can effectively eliminate the sensor negative impacts on building energy consumption and thermal comfort. A study [21] applied fault mitigation techniques for sensors (read back for sensor readings and nearest neighbor monitoring for fault sensor correcting), which demonstrated up to 38% improvement in energy consumption and up to 75% improvement in thermal comfort. The sensor faults include stuck-at fault, spike-and-stay (SAS) fault with negative spike, spike-and-stay (SAS) fault with positive spike, single-sample-spike (SSS) fault with negative spike, and single-sample-spike (SSS) fault with positive spike.

However, current literature studies assume sensor fault or errors are constant [5,9,15,22,23]. In real conditions, sensor fault magnitude could evolve or develop over time, which is often observed from field measurements. This is the essence of incipient sensor faults. This is also the main purpose of this study. How to address such an issue is relying on correct modeling of sensor errors. Another research gap is that there was no study proposing a sensor impact evaluation framework. Available studies use their own sensor impact evaluation platform.

The structure of this study is organized as follows: Section 2 summarizes the sensor impact and evaluation framework, which is the methodology; Section 3 describes the surrogate model; Section 4 describes the uncertainty analysis; Section 5 describes the sensitivity analysis; and Section 6 provides conclusions.

2. Methodology

This study aimed to systematically investigate incipient sensor faults for building control performance. The US Department of Energy's Oak Ridge National Laboratory's (ORNL's) two-story Flexible Research Platform (FRP-2) building was used to study the sensor fault impacts. It is a two-floor building with five zones on each floor. The cooling is from rooftop unit (RTU). The heating is from a gas heating coil and VAV electric coils. The control strategy for single-duct variable air volume (VAV) terminal boxes and the air

handling unit (AHU) is implemented based on the control logics from ASHRAE Guideline 36-2018, High-Performance Sequences of Operation for HVAC Systems [24].

A sensor-impact oriented framework is proposed for this purpose. The framework is comprised of (1) a physics-based emulator integrated with sensor faults, control sequences, and building/HVAC models; (2) large-scale simulations for sensor error samplings to the controls on the cloud; (3) a surrogate model development based on cloud simulation results for sensitivity analysis; and (4) sensitivity and uncertainty analyses for the sensors and desired outputs (e.g., energy consumption, thermal comfort).

This study is based on EnergyPlus platform through building energy models. The overall workflow is illustrated in Figure 1. Cloud simulation was used to quicken the 3600 simulation cases, using a stochastic approach. The uncertainty and sensitivity analyses are based on simulation data from cloud simulation. The building model details are not presented here. Interested readers, please refer to the recent publications on the building [25].

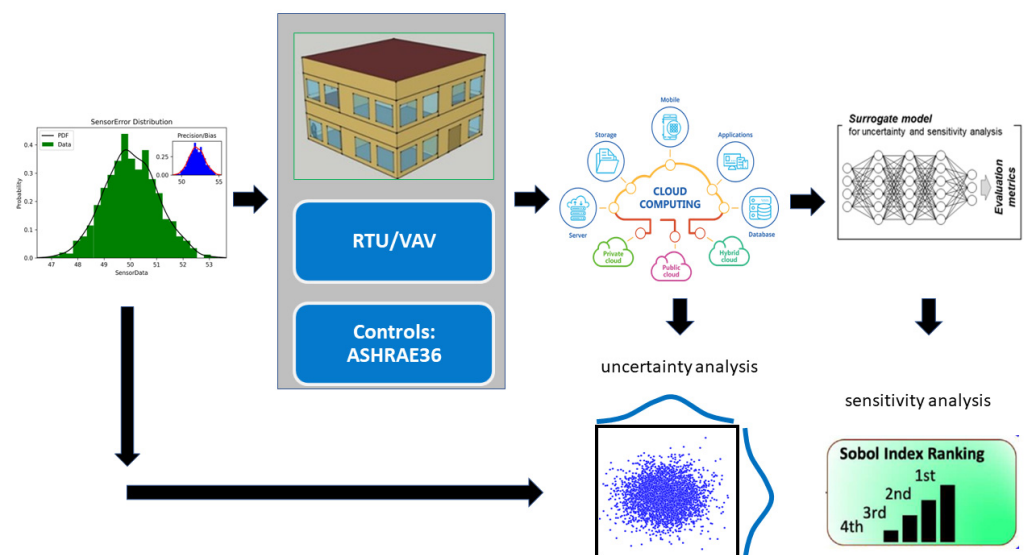


Figure 1. Sensor impact and evaluation framework.

The pseudo code for the sensor fault injection and simulation is shown in Figure 2. The pseudo code follows the basic flowchart in Figure 1, which demonstrates the basic principle of how to implement the sensor impact analysis.

```
for time in range(0, 365*24*60):
    sensor_readings = get_building_states(energyplus_api)
    sensor_err_bias = generate_sensor_err_bias()
    sensor_err_precision = generate_sensor_err_precision()
    sensor_err_tot = sensor_err_bias + sensor_err_precision
    overwrite_sensor_readings(energyplus_api)
    calc_hvac_energy_consumption(energyplus_api)
```

Figure 2. Pseudo code for sensor fault injection and simulation.

2.1. Sensor Sets

Based on extensive literature reviews, 34 sensors were identified. They are typical sensors used to operate RTU and variable air volume (VAV) systems in small to medium office buildings. The sensors were prioritized based on the severity of indoor air (IA) temperature impacts, which can significantly affect energy efficiency and occupant thermal comfort. The identified sensors are frequently used in commercial buildings. They are listed in Table 1.

Table 1. Comprehensive sensor list.

Location	Measurement	Priority	Location	Measurement	Priority
Room	IA temperature	1	RTU	OA CO ₂	4
Room	IA humidity	3	RTU	OA flow rate	3
Room	IA CO ₂	4	RTU	SA temperature	1
Room	Lighting condition	5	RTU	SA humidity	3
Room	Occupancy	5	RTU	SA CO ₂	4
VAV box	SA temperature	1	RTU	SA flow rate	3
VAV box	SA humidity	3	RTU	RA temperature	2
VAV box	SA flow rate	1	RTU	RA humidity	3
Main duct	Static pressure	2	RTU	RA CO ₂	4
Exhaust fan	EA temperature	4	RTU	RA flow rate	3
Exhaust fan	EA humidity	4	RTU	MA temperature	2
Exhaust fan	EA flow rate	4	RTU	MA humidity	3
Exhaust fan	EA CO ₂	4	RTU	MA CO ₂	4
Other	Plug load	5	RTU	MA flow rate	3
Other	Lighting load	5	RTU	Refrigerant temperature	5
RTU	OA temperature	1	RTU	Refrigerant pressure	5
RTU	OA humidity	3	RTU	Refrigerant flow rate	5

SA = supply air; EA = exhaust air; OA = outdoor air; RA = return air; MA = mixing air; IA = indoor air.

Based on the actual HVAC system configuration of the FRP-2 building, five sensor types were selected for the following reasons: (1) Those sensors were closely matching with the selected control logics. Different control logics might need different sets of sensors; (2) the IA temperature is the most important variable to be controlled to meet the heating and cooling set point temperatures; (3) the VAV box supply air (SA) temperature and SA flow rates (SAFs) directly affect the IA temperature from the control perspective; (4) RTU system-level operation also directly affects the VAV box operations; and (5) RTU outdoor air (OA) temperature (OAT) and SA temperature (SAT) are important for determining system-level energy consumption. The sensor types are listed in Table 2. The specification of the selected sensors is described in Table 3.

Table 2. Selected sensor list.

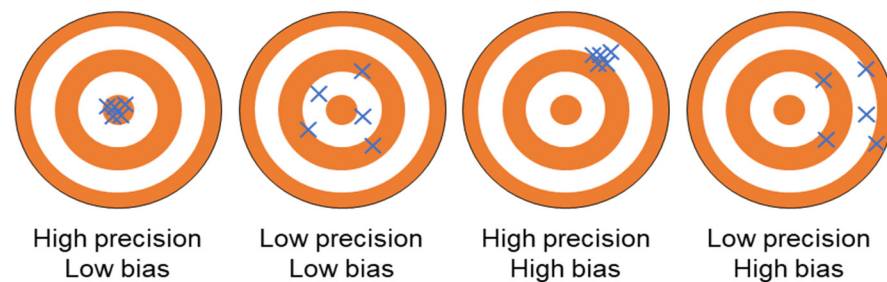
Location	Measurement	Priority	Note
Room	IA temperature	1	IA temperature
VAV box	SAT	1	VAV box SAT
VAV box	SAF	1	VAV box SAF
RTU	OAT	1	OAT
RTU	SAT	1	SAT

Table 3. Specification of the selected sensor.

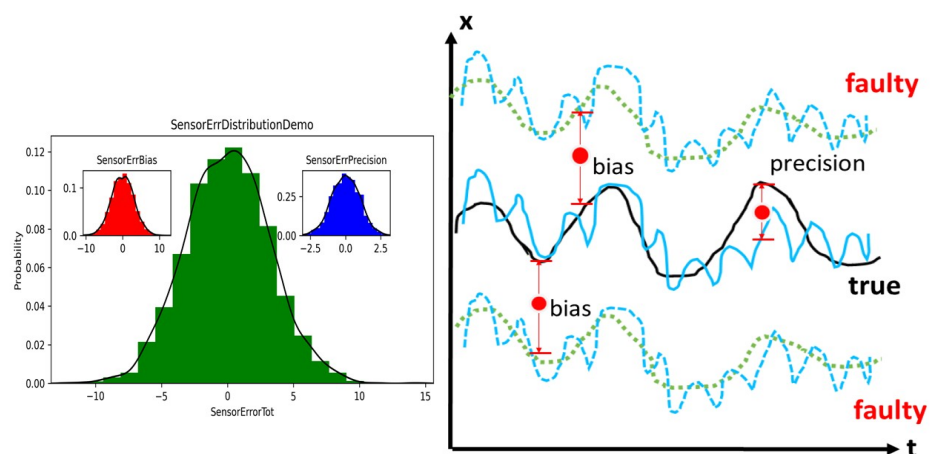
Measured Data	Range
Outdoor air temperature	−50~100 °C
Indoor air temperature	
Supply air temperature	
Supply airflow rate	0~15.24 m/s

2.2. Sensor Errors

Available literature assumes fixed or constant sensor errors. Here, we proposed the incipient sensor error as bias error and precision (random) error. This research team identified two components for sensor faults [4]: precision and bias. Precision is used to measure how precise the sensor reading is from the true reading because of measuring noise. Bias is used to measure how far the sensor reading is from the true reading because of system bias. Figure 3 shows a diagram for precision and bias. A typical characteristic of incipient faults is that the fault magnitude might change slowly with time and effects on control performance might go unnoticed.

**Figure 3.** Sensor error component.

For a sensor, an ideal reading (or true reading) exists at a given time step, as shown by the black line in Figure 4. The bias error is the system deviation from the ideal readings, as shown by the green dotted lines in Figure 4. The precision error is the random deviation or noise from the average sensor readings, as shown by the blue dashed lines in Figure 4.

**Figure 4.** Sensor error diagram.

The mathematical expression of such a fault profile is given as

$$X_f(t) = X_o(t) + X_{bias}(t) + X_{precision}(t) \quad (1)$$

where X_f is the fault reading, X_o is the ideal reading (no fault), X_{bias} is the bias error, and $X_{precision}$ is the precision error.

The bias error is a normal distribution with a certain standard deviation. The expression is given as

$$X_{bias}(t) = N(0, \sigma_{bias}) \quad (2)$$

The precision error is also a normal distribution with a certain standard deviation. The expression is given as

$$X_{precision}(t) = N(0, \sigma_{precision}) \quad (3)$$

where σ_{bias} is the standard deviation of bias error and $\sigma_{precision}$ is the standard deviation of precision error.

The sensor errors were incorporated based on the emulator of EnergyPlus and Python EMS. Due to the technical difficulties from larger airflow sensor errors, the airflow sensor errors need to be within an effective range. The standard deviations for the five types of selected sensors are shown in Table 4.

Table 4. Standard deviation of selected sensor errors.

Location	Measurement	Bias	Precision
Room	IA temperature (°C)	1	0.1
VAV box	SAT (°C)	1	0.1
VAV box	SAF (m ³ /s)	0.005	0.0005
RTU	OAT (°C)	1	0.1
RTU	SAT (°C)	1	0.1

2.3. Control Logic for RTU and Single-Duct VAV System (ASHRAE Guideline 36)

The installed HVAC systems in the FRP-2 building are RTUs, in which cooling is from a direct expansion cooling coil and heating is from a gas heating coil. The FRP-2 building has 10 conditioned zones. Each conditioned zone is served by a VAV box with an electricity reheat coil. The air handling unit (AHU) connects all the zone VAV boxes and the RTU. Control logic from ASHRAE Guideline 36-2018, High-Performance Sequences of Operation for HVAC Systems [24], was developed for the RTUs and VAV boxes.

1. AHU: Trim and Respond (T&R) Set Point Logic

The first control logic is the T&R set point logic for the AHU. T&R logic resets set points of the pressure, temperature, or other variables on the AHU or plant side. T&R logic reduces the set point at a fixed rate until the zone thermal comfort is no longer satisfied; then, it generates the request. The set point is increased in response to a sufficient number of requests. By adjusting the importance of each zone's requests, the critical zones will always be satisfied. If there are not a sufficient number of requests, then the set point decreases at a fixed rate.

The term “request” refers to a request to reset a static pressure or temperature set point generated by downstream zones or AHUs. These requests are sent upstream to the AHU or plant that supplies the zone or area that generated the request. For more details of Trim & Respond logic, please refer to the documents of [24,26].

T&R control was used to reset the RTU SA set point temperature in the emulator. When the OAT was higher than the maximum OAT (21 °C), the RTU SAT was set to the minimum RTU SA set point temperature (12 °C). When the OAT was lower than the minimum OAT (16 °C), the RTU SAT was set to the maximum RTU SA set point temperature (18 °C). If the OAT was between the minimum and maximum OAT when the OAT was increased, then the RTU SAT was linearly increased from the minimum RTU SA set point temperature to the maximum RTU SA set point temperature. For T&R control, as ASHRAE Guideline 36 describes, fewer than two requests were ignored.

2. VAV box control logic

The VAV box control is the second control logic applied to the emulator. Figure 5 shows the control logic for the VAV box from ASHRAE Guideline 36. The control logic has three sections, which correspond to the heating mode, cooling mode, and dead-band, and it uses the heating loop demand concept. Heating loop demand is the ratio (as a percentage) of the actual required heating load of the VAV box to the size of the VAV box. Equation (4) describes how to calculate the heating loop demand.

$$\text{Heating loop demand} = \frac{\text{Heating load of the VAV box}}{\text{Capacity of the VAV box}} \times 100 \quad (4)$$

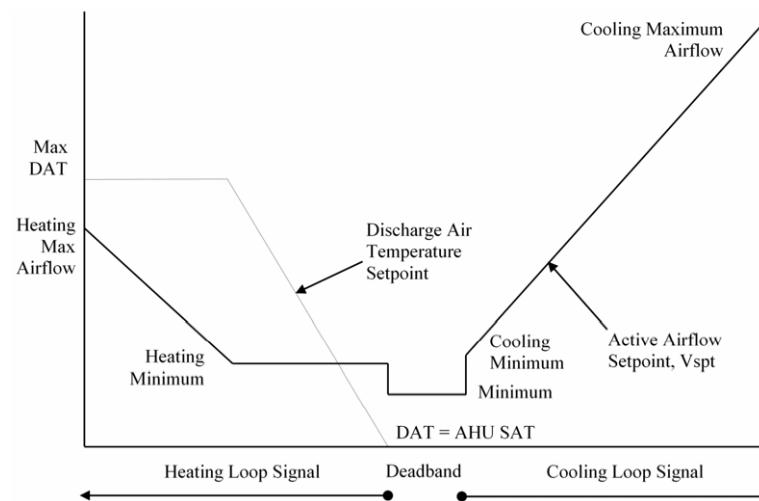


Figure 5. Control logic for VAV box from ASHRAE Guideline 36 [24,26].

The detailed logics are threefold:

- a. In the heating mode, when the heating loop is less than or equal to 50%, the discharge air (DA) set point temperature of the VAV box is increased from the RTU SAT to the maximum DA set point temperature of the VAV box, and the minimum SAF is maintained. When the heating loop is greater than 50%, if the DA temperature of the VAV box is greater than the IA temperature plus 3 °C, then the SAF of the VAV box is increased from the minimum SAF to the maximum SAF while maintaining the maximum DA set point temperature of the VAV box;
- b. In the cooling mode, the DA temperature of the VAV box is the same as the RTU SAT because no option exists to decrease the SAT using the VAV box. Therefore, VAV box control is linked with T&R control in the cooling season, when the VAV box control must be considered the RTU SAT. The four cooling SA set point temperature reset requests are as follows:
 - If the IA temperature exceeds the indoor cooling set point temperature by 3 °C for 2 min and after the suppression period resulting from an RTU SA set point temperature change via the T&R control, then send three requests;
 - Else, if the IA temperature exceeds the indoor cooling set point temperature by 2 °C for 2 min and after the suppression period resulting from an RTU SA set point temperature change via the T&R control, then send two requests;
 - Else, if the cooling loop is greater than 95%, then send one request until the cooling loop is less than 85%;
 - Else, if the cooling loop is less than 95%, then send no request.

In terms of the SAF in the cooling season, the SAF of the VAV box is increased from the minimum SAF to the maximum SAF as the cooling loop is increased;

- c. In the dead-band mode, when neither heating nor cooling are needed, the SAF is set to the minimum SAF, and the DA temperature of the VAV box is set to the RTU SAT.

The overall control logic is shown in Figure 6.

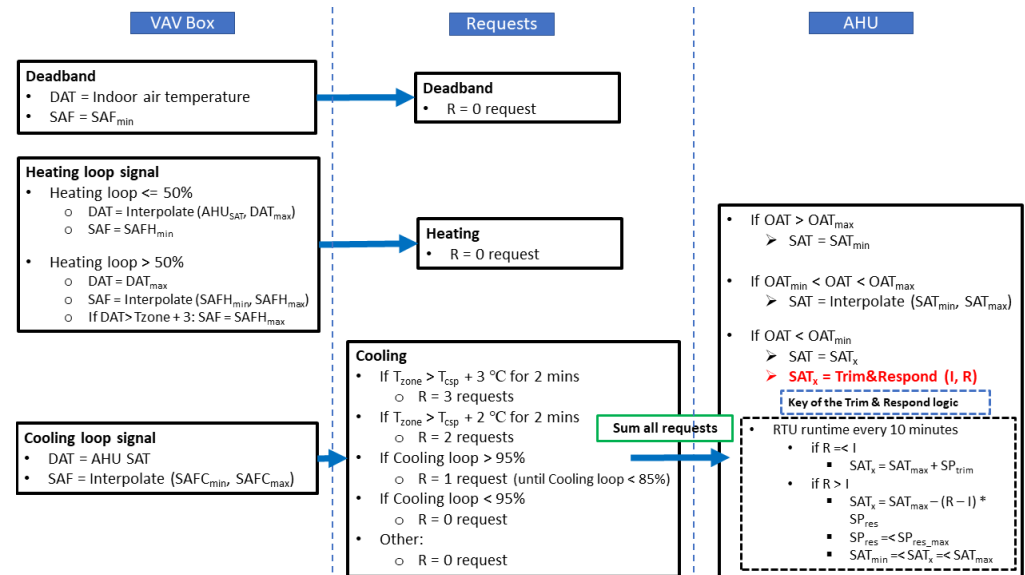


Figure 6. Overall control logic for VAV box and AHU. (DAT: discharge air temperature; SAFH: supply air flow rate for heating; SAFC: supply air flow rate for cooling; R: number of requests; I: ignored responses; SP: respond amount.)

2.4. Large-Scale Simulation

The large-scale simulation was based on a commercial cloud platform, Microsoft Azure. In total, 3600 cases were simulated on the cloud. The inputs were the sensor errors incorporated into the five selected sensors for the FRP-2 building emulator, as shown in Table 2. The sensor errors were obtained using normal distribution samplings. EnergyPlus internal programming limits caused simulation crashes when larger sensor errors were incorporated. The standard deviations of sensor errors were based on multiple trials. The thresholds were based on engineering experience, domain knowledge, and actual RTU- and zone-level sensor ideal readings. The outputs were the target variables for energy consumption and thermal comfort, such as fan electricity consumption and reheat coil electricity energy in the VAV box.

The basic diagram is shown in Figure 7. The basic workflow is as follows:

- (1) A Python script was developed to generate 3600 simulation input data files (IDF files). Each IDF file was associated with a Python class of sensor errors through Python EMS. During the simulation, at each time step, a new sensor error (including bias and precision) was injected into the ideal sensor readings from EnergyPlus;
- (2) After 3600 cases were generated, they were uploaded to the Azure cloud platform;
- (3) In the Azure cloud platform, a bash script selected the appropriate virtual machine configurations (e.g., memory and hard drive, as shown in Table 4) and a number of virtual machines. The team's subscription included 300 nodes (virtual machines);
- (4) The Azure cloud provided a job scheduler, which automatically distributed all 3600 cases across 300 nodes;
- (5) The simulation ran automatically until all cases were accomplished;
- (6) Finally, all the results were selected to set up the data sets (inputs and outputs) to create the black-box models.
- (7) The configuration for the cloud is shown in Table 4.

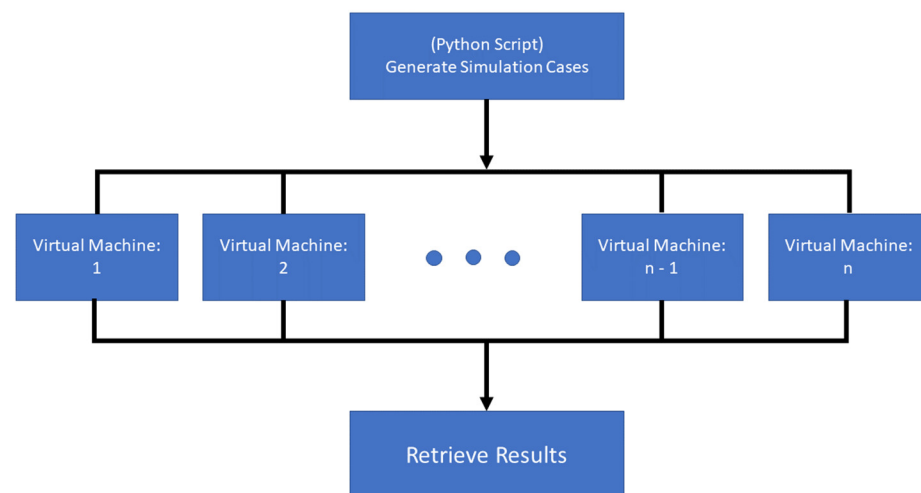


Figure 7. Cloud simulation workflow.

A total of 300 nodes were used for the cloud simulation, in which each node is a standard node: 16 cores, 64 GB memory, and 600 GB storage capacity. The total simulation time is about 9 h.

The sensor errors were sampled using a normal distribution for each time step. The sensor readings from EnergyPlus used the sensor errors to form the faulty sensor readings. The faulty sensor readings were used as inputs to control sequences to calculate new set points. These new set points were used to control the performance of buildings. Ultimately, the simulated energy consumption and thermal comfort were different from the results obtained using the ideal sensor readings.

2.5. Other Aspects

In order to ensure that the simulation results are correct, there are a few extra explanations summarized below.

- (1) The baseline model was calibrated with the actual components and systems within the FRP2 building at ORNL campus. The input values for the HVAC system are from the measurement and nameplate values. The simulation results demonstrated the consistency between model and measurements [25];
- (2) The simulation cases have a total of 3600 sets. Each case matches with a sensor error module. In each timestep, the sensor error value will be injected into the model following the sensor error components (bias and precision). The energy consumption differences were easily calculated between baseline case and sensor-error case, which was caused by the sensor errors. If sensor errors were made to be zero all through the simulation timesteps, the same energy consumption was obtained with baseline model;
- (3) We analyzed the results and see that they are reasonable for sensor errors. For example, (a) when we increase the sensor error to the zone temperature for cooling mode (lower zone temperature than it is supposed to be), we can see the energy consumption increasing. This is because the building model thinks it needs more cooling energy to meet the cooling setpoints. (b) When we increase the sensor error to the zone temperature sensor for heating mode (higher zone temperature than it is supposed to be), we can see the energy consumption decreasing. This is because the building model thinks it needs less heating energy to meet the heating setpoints;
- (4) To explain in detail, the sensor error in this study followed the normal distribution (Figure 4) and the sensor error range was calculated by bias sensor error plus precision error. For example, if the standard deviation of sensor error of the temperature sensor is 1 °C, the temperature sensor error range is within −3 °C and +3 °C with a probability of 99.76%. Similarly, the probability of sensor error range between −1 °C and +1 °C is about 68%. The probability of sensor error range within −2 °C and +2 °C is about

95.4%. The extreme cases are within 0.24% of scenarios on the two ends. Therefore, the differences (numbers) mentioned above occur when the sensor error is the largest (either positive or negative values).

3. Surrogate Model

To accomplish sensitivity analysis, the surrogate model was developed based on cloud simulations. The long short-term memory (LSTM) model was selected because it includes previous time step input impacts. These impacts are important because inertia phenomena exist in buildings. The LSTM model internally reflects thermal inertia.

3.1. LSTM Setup

The LSTM model is a neural network model suitable for time-series forecasting. For building energy simulations, the results are time-series variables. The thermal state of buildings at previous time steps has certain impacts on the later time steps. The main purpose of the LSTM model is to find the mapping of inputs and outputs. Figure 8 shows that the input variables were transformed into multiple routes as a way of including previous states' impacts. Detailed mathematics are not included here because the goal was to use the LSTM model to make a black-box model. Many publications already investigated the mathematical details, such as the inventor of LSTM algorithm [27].

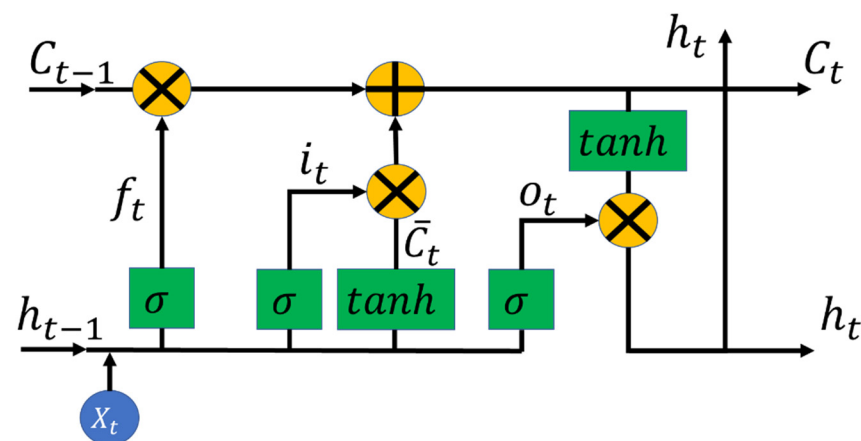


Figure 8. LSTM cell structure.

3.2. Training and Setting

The whole data set was divided into a training data set (80% of total) and a validation data set (20% of total). The training data set was used to learn the weights of input variables to output variables. The validation data set was used to test the accuracy of the surrogate model prediction from the emulator output variables. The data sets were shuffled to avoid the input data internal impacts. The root mean square error was used to quantify the modeling accuracy:

$$RMSE = \sqrt{\frac{\sum_1^N (y_i - \hat{y}_i)^2}{N}} \quad (5)$$

where $RMSE$ is the root mean square error, y_i is the emulator output variable, \hat{y}_i is the surrogate model output variable, and N is the total number of variables in the prediction.

3.3. Input/Output Variables

The surrogate model established the mapping relationship between input and output variables. The input variables were based on the FRP-2 EnergyPlus models. A detailed list of variables is provided in Table 5.

Table 5. Input variables.

Variable Name	Quantity
OAT	1
OA relative humidity	1
OA pressure	1
Wind speed	1
Wind direction	1
Horizontal infrared radiation rate	1
Diffuse solar radiation rate	1
Direct solar radiation rate	1
Lighting energy	1
Internal heat gains: equipment	1
People activity	1
SensorBias: AHU OAT	1
SensorPrecision: AHU OAT	1
SensorTotalError: AHU OAT	1
SensorBias: AHU SAT	1
SensorPrecision: AHU SAT	1
SensorTotalError: AHU SAT	1
SensorBias: zone VAV SAF	10
SensorPrecision: zone VAV SAF	10
SensorTotalError: zone VAV SAF	10
SensorBias: zone VAV SAT	10
SensorPrecision: zone VAV SAT	10
SensorTotalError: zone VAV SAT	10
SensorBias: zone air temperature	10
SensorPrecision: zone air temperature	10
SensorTotalError: zone air temperature	10
Total	107

The output variables were also based on FRP-2 EnergyPlus simulation models. A detailed list of output variables is provided in Table 6.

Table 6. Output variables.

Variable	Quantity
Fan electricity rate (W)	1
Main cooling coil sensible cooling rate (W)	1
Main cooling coil electricity rate (W)	1
Main heating coil heating rate (W)	1
Zone air sensible heating rate (W)	10
Zone air sensible cooling rate (W)	10
Zone air temperature (°C)	10
Zone predicted percentage dissatisfied (%)	10
VAV box reheat energy (W)	10
Total	54

3.4. Workflow for Surrogate Model Training

In total, 3600 simulation cases were simulated on the cloud. Each case generated 1.3 GB of data with 1 min time resolution. A 4.7 TB data set was obtained. To expedite the surrogate model training, a distributed machine learning framework was used. The workflow is shown in Figure 9. Through the cloud, 32-core machines were used. The 3600 cases were divided into 20 groups, or cores, with each group responsible for 180 cases. After all training was completed for each group, the final model parameters were obtained by averaging model parameters from the 20 groups of training.

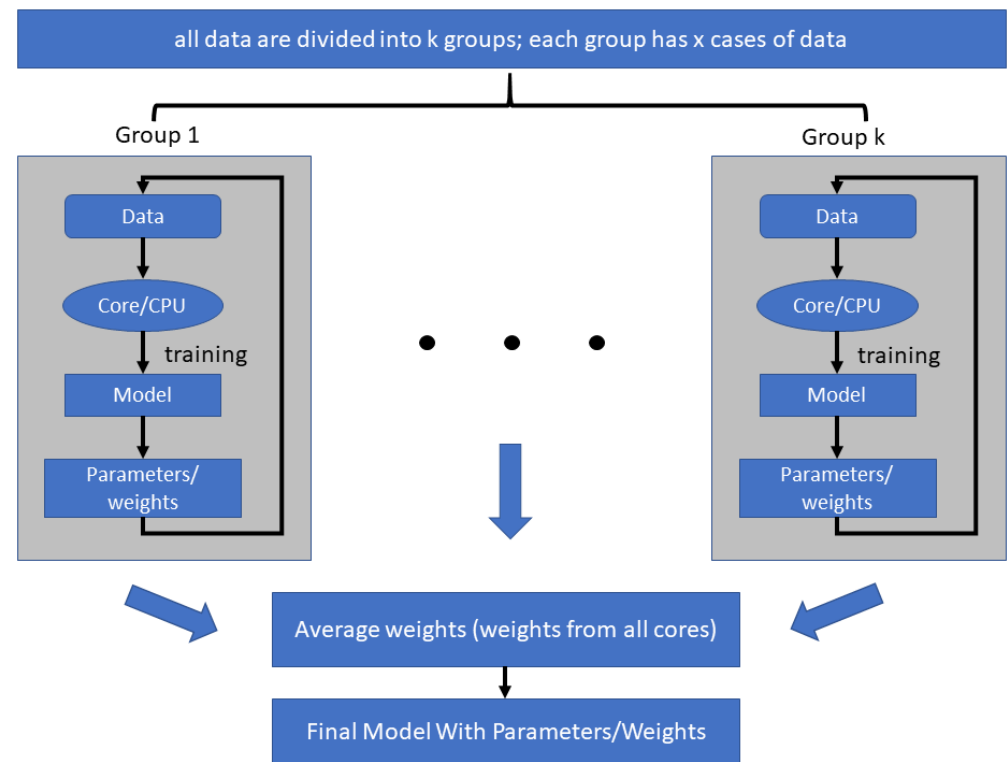


Figure 9. Distributed training of surrogate models.

4. Uncertainty Analysis

4.1. Uncertainty Analysis Setup

Uncertainty analysis assesses the uncertainty of output/target variables in the model in which the inputs are under uncertainty samplings. The purpose of this uncertainty analysis was to identify how output variables were distributed in response to uncertainties of input values. Generally, a wider distribution of output variables corresponds with increased sensitivity of the output variables to the input variables. For this uncertainty analysis, the large-scale simulation (3600 cases) was conducted on a cloud platform. Figure 10 illustrates the overall process of the uncertainty analysis. The standard deviations of input values (sensor errors) of the uncertainty analysis are listed in Table 5 and selected output variables are listed in Table 6. Before the uncertainty analysis, HVAC system controls based on ASHRAE Guideline 36 [24] were applied using the Python EMS function, as described in Section 2.3. Input values for the system control were obtained from the simulation results; then, the total sensor error was added to the HVAC system control. Using the physics-based emulator, 3600 cases were generated. The results are described in Section 4.2.

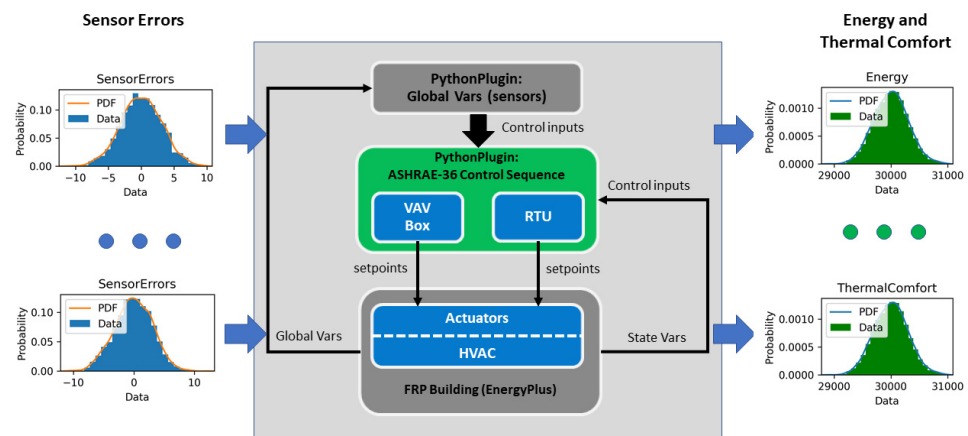


Figure 10. Uncertainty analysis process.

4.2. Uncertainty Analysis Results

For large-scale simulations, each case generated the aggregated energy consumption: site energy, heating energy, cooling energy, and fan energy. The baseline results are 304,083 kBTU (site energy), 60,081 kBTU (heating energy), 105,482 kBTU (cooling energy), and 50,422 kBTU (fan energy). Figure 11 demonstrates the energy distributions under sensor fault and baseline energy items. It shows that the energy consumption varies drastically from the baseline cases, due to the sensor errors.

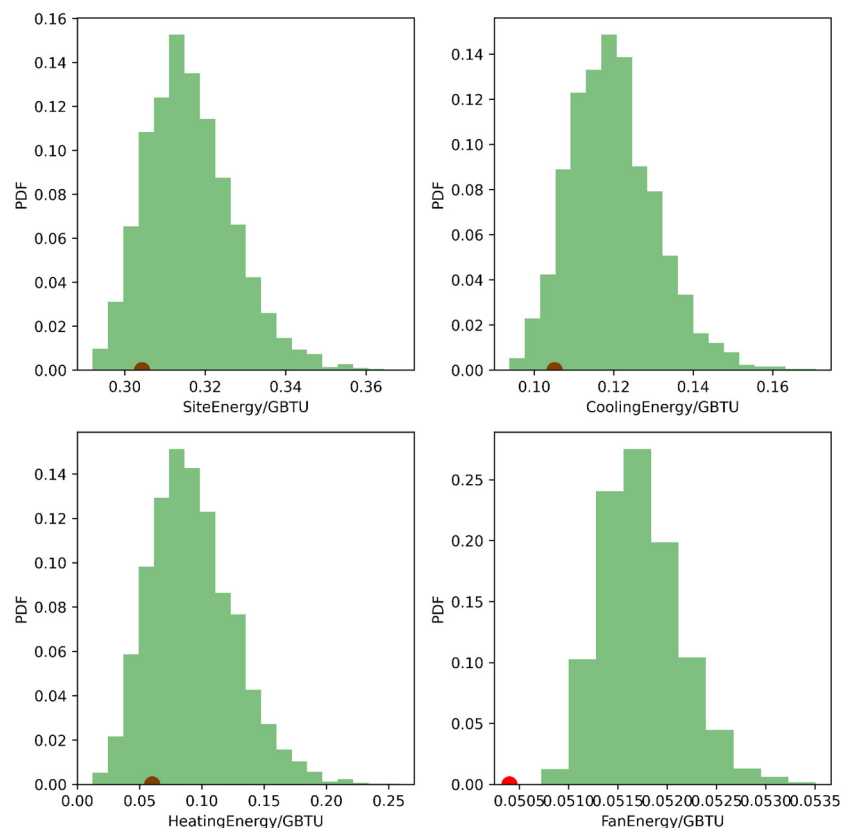


Figure 11. Energy distributions and baseline energy items.

Figure 12 shows the site energy consumption with averaged sensor error distributions. The top left shows the AHU OAT and SAT sensor errors with site energy consumption. The top right shows the VAV box SAT sensor errors and site energy consumption. The bottom left shows the zone temperature sensor errors with site energy consumption.

The bottom right shows the VAV box SAF sensor errors with site energy consumption. From the distributions, the sensor errors show normal distributions instead of a linear relationship. The site energy consumption was 294,000~359,000 kBtu/year based on the distribution of sensor total errors. The change of total site energy consumption was 65,000 kBtu/year, which is 21.4% of the average site energy consumption (340,083 kBtu/year). The site energy impacts could go -3.3% lower or 18.1% higher, compared with baseline. The above energy patterns are a comprehensive demonstration of sensor errors. The underlying logics are: (1) For negative sensor errors under cooling mode, zone temperature sensors would deliver smaller sensor readings to the controls. This could make the control systems call on a larger supply air flow rate or supply air temperature to meet the zone thermal setpoints. This could cause more energy consumption for the cooling coils. (2) For positive sensor errors under cooling mode, zone temperature sensors might deliver higher sensor readings to the controls. This could fool the control system to call on a smaller supply air flow rate or supply air temperature. This will cause the zone to be too hot, subject to thermal comfort issue. (3) For negative sensor errors under heating mode, the zone temperature sensor reading would be smaller, which fools the control system to increase the supply air temperature or supply air flow rate to maintain the zone temperature setpoints. This could cause more heating energy consumption from the heating coils. (4) For positive sensor errors under heating mode, the zone temperature sensor reading would be higher, which leads the control system to decrease supply air temperature or supply air flow rate to maintain the thermal setpoints. This would cause less heating energy demands from the heating coils. Since the sensor errors evolve each time step, this adds more complexity to the control actions, which lead to complicated energy consumption patterns.

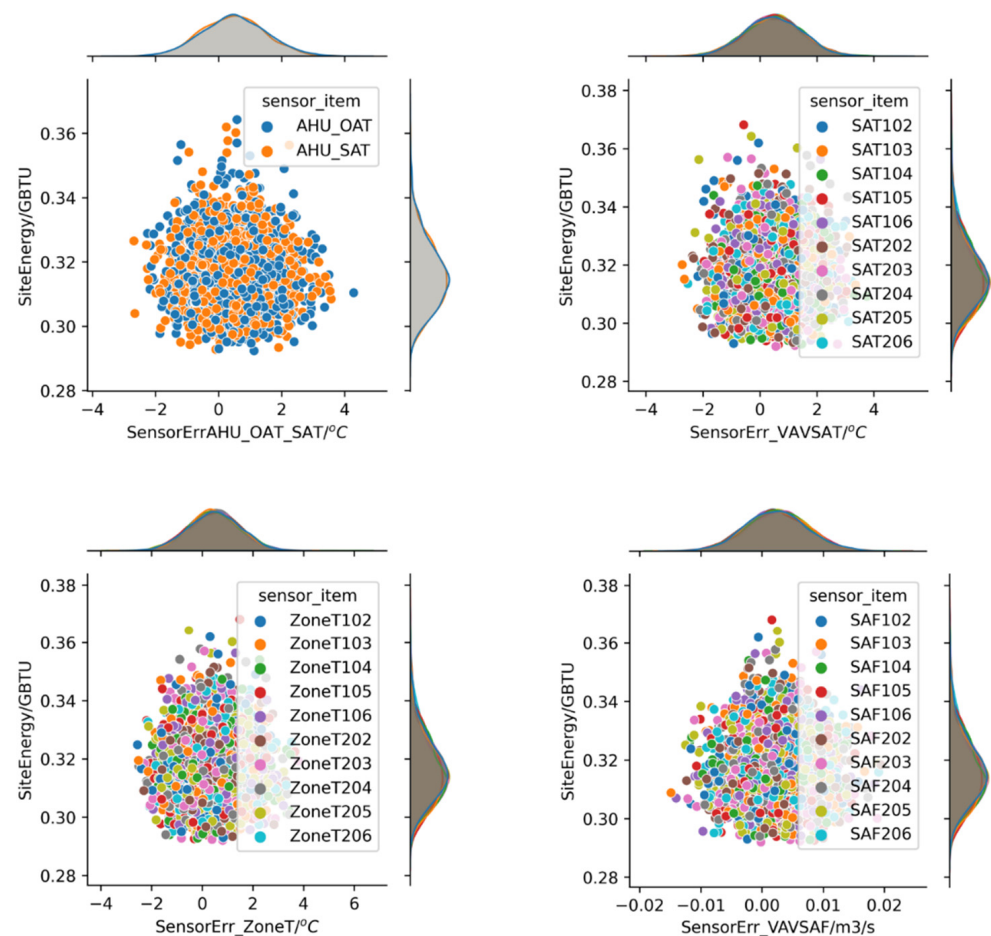


Figure 12. Site energy and sensor errors.

Figure 13 shows the total heating energy consumption with averaged sensor error distributions. The top left shows the AHU OAT and SAT sensor errors with heating energy consumption. The top right shows the VAV box SAT sensor errors and heating energy consumption. The bottom left shows the zone temperature sensor errors with heating energy consumption. The bottom right shows the VAV box SAF sensor errors with heating energy consumption. From the distributions, the sensor errors show normal distributions instead of a linear relationship.

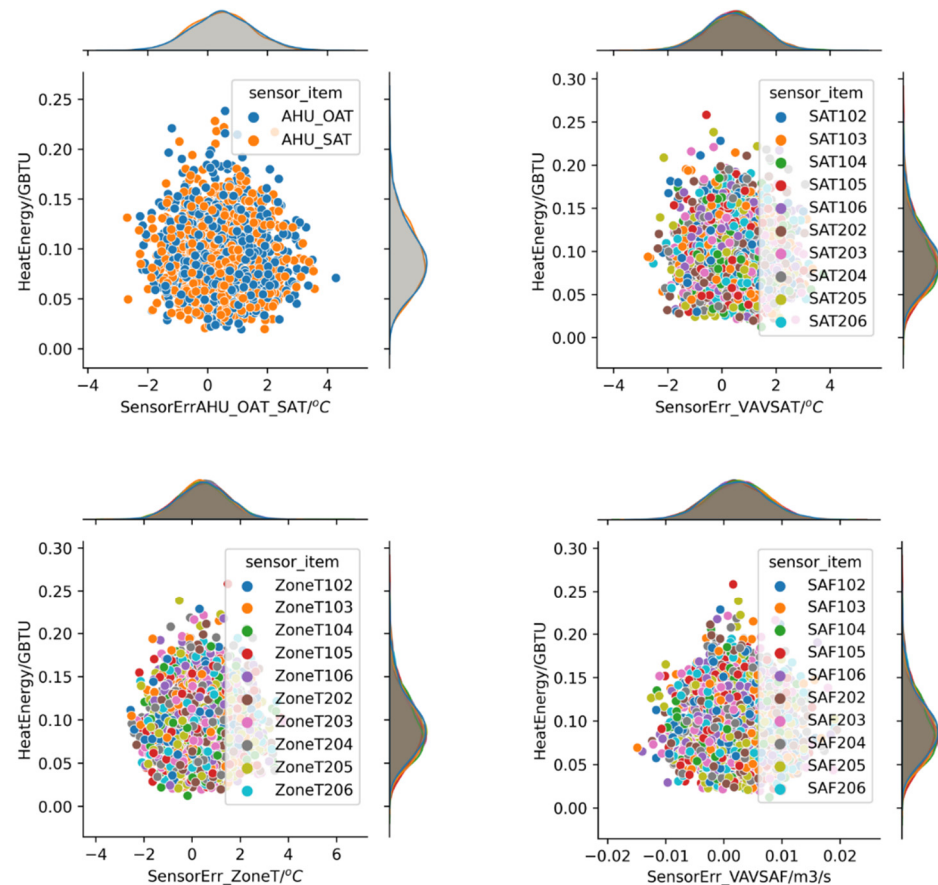


Figure 13. Heating energy and sensor errors.

The heating energy consumption was 20,130~249,000 kBtu/year based on the distribution of sensor total errors. The change of total heating energy consumption was 228,870 kBtu/year, which is 380% of the baseline heating energy consumption (23,265 kBtu/year). The heating energy impacts could go −66.5% lower or 314.4% higher, compared with baseline.

Figure 14 shows the total cooling energy consumption with averaged sensor error distributions. The top left shows the AHU OAT and SAT sensor errors with cooling energy consumption. The top right shows the VAV box SAT sensor errors with cooling energy consumption. The bottom left shows the zone temperature sensor errors with cooling energy consumption. The bottom right shows the VAV box SAF sensor errors with cooling energy consumption. From the distributions, the sensor errors show normal distributions instead of a linear relationship. The cooling energy consumption was 93,320~174,000 kBtu/year based on the distribution of sensor total errors. The range of total cooling energy consumption change was 80,680 kBtu/year, which is 76.5% of the baseline cooling energy consumption (133,660 kBtu/year). The cooling energy impacts could go −11.5% lower or 65.0% higher, compared with baseline.

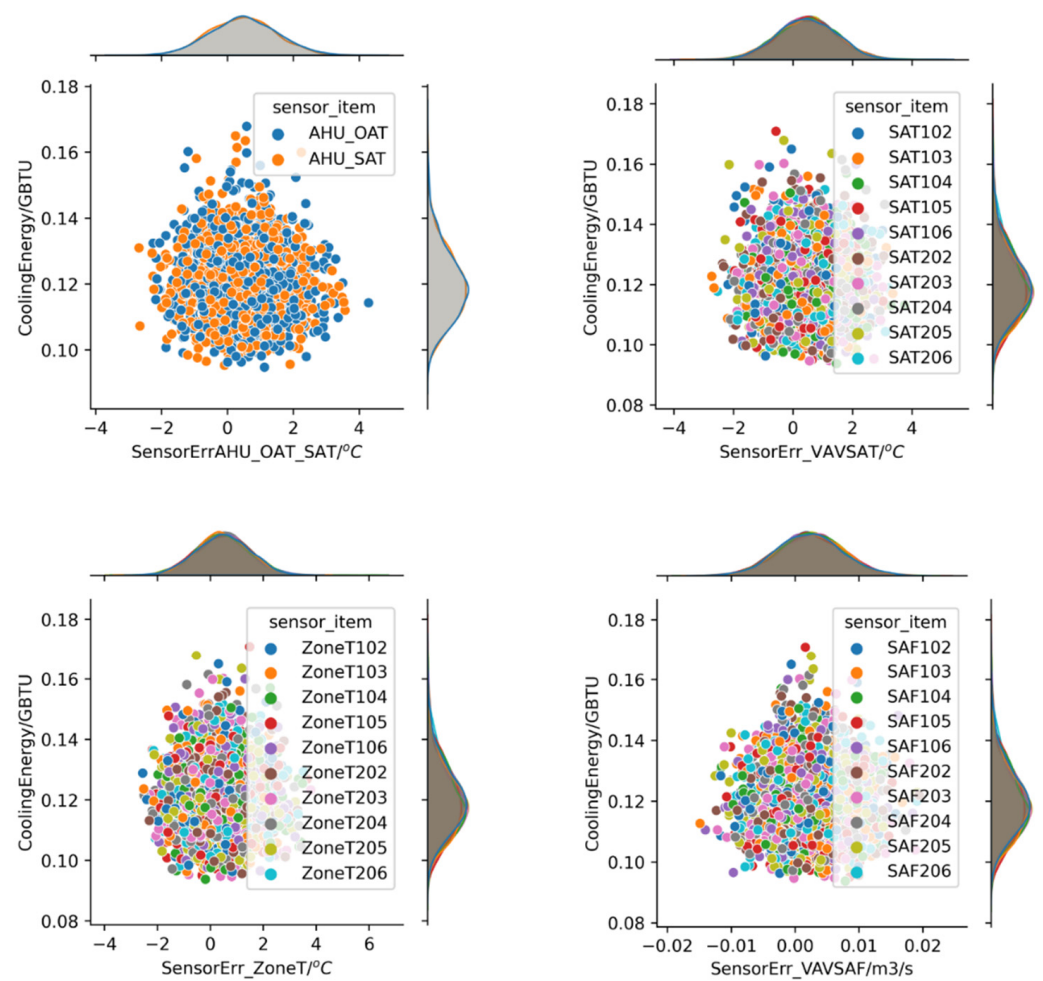


Figure 14. Cooling energy and sensor errors.

Figure 15 shows the total fan energy consumption with averaged sensor error distributions. The top left shows the AHU OAT and SAT sensor errors with fan energy consumption. The top right shows the VAV box SAT sensor errors with fan energy consumption. The bottom left shows the zone temperature sensor errors with fan energy consumption. The bottom right shows the VAV box SAF sensor errors with fan energy consumption. From the distributions, the sensor errors show normal distributions instead of a linear relationship.

The fan energy consumption was 50,501~53,900 kBtu/year based on the distribution of sensor total errors. The change of total fan energy consumption was 3399 kBtu/year, which is 6.7% of the baseline fan energy consumption (50,422 kBtu/year). The fan energy impacts could go 0.15% lower or 6.9% higher, compared with baseline.

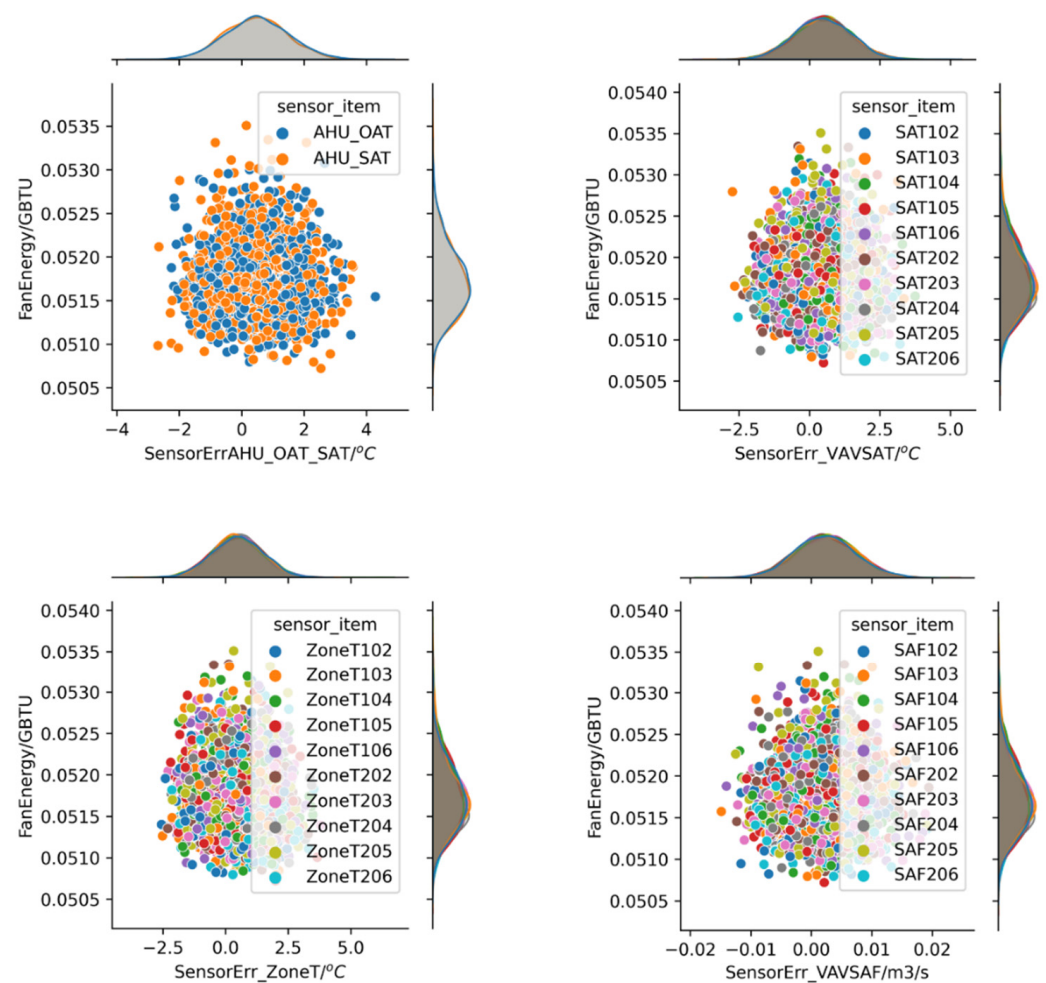


Figure 15. Fan energy and sensor errors.

5. Sensitivity Analysis

5.1. Sensitivity Analysis Principle

The sensitivity analysis identified which sensor errors have stronger impacts on energy consumption and thermal comfort. A ranking of sensor error impacts was obtained using sensitivity analysis index values. Sensitivity analysis can be performed in various ways, including through local and global approaches [28,29]. Different methods have certain strengths and drawbacks. As a preliminary exploration, this project applied the Sobol method [28] to calculate the sensitivity index.

The principle is described as

$$Y = f_0 + \sum_{i=1}^d f_i(X_i) + \sum_{i<j}^d f_{ij}(X_i, X_j) + \cdots + f_{1,2,\dots,d}(X_1, X_2, \dots, X_d) \quad (6)$$

where Y is one of the interested model outputs, X_i is the model input with uncertainty, d is the total number of model inputs with uncertainties, f_0 is the constant, f_i is the function of X_i , and f_{ij} is the function of X_i and X_j .

The sensitivity index is given as

$$S_i = \frac{V_i}{Var(Y)} \quad (7)$$

where V_i is the variance with respect to variable input X_i and $Var(Y)$ is the total variance of the output variable Y .

The definitions of these variances are

$$V_i = \text{Var}_{X_i}(E_{X_{\sim i}}(Y|X_i)) \quad (8)$$

$$\text{Var}(Y) = \sum_{i=1}^d V_i + \sum_{i<j}^d V_{ij} + \dots + V_{12\dots d} \quad (9)$$

where, $\sim i$ means all the input variables except X_i .

Note that

$$\sum_{i=1}^d S_i + \sum_{i<j}^d S_{ij} + \dots + S_{12\dots d} = 1 \quad (10)$$

The workflow for the sensitivity analysis is shown in Figure 16.

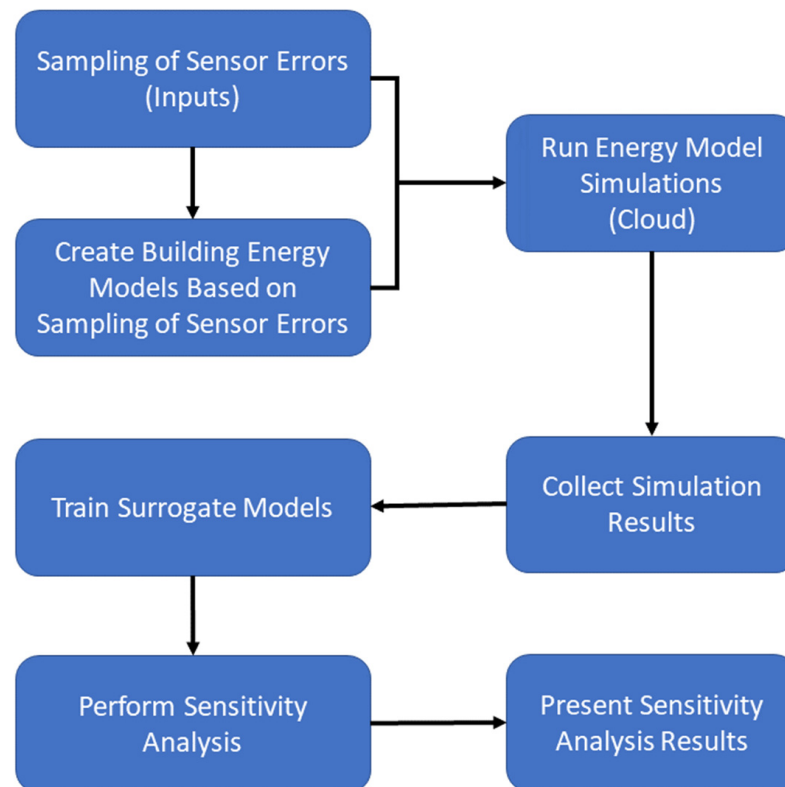


Figure 16. Sensitivity analysis flowchart.

5.2. Sensitivity Analysis Results

Based on the simulation results, AHU- and zone-level sensitivity analyses were performed. The results are presented in the following subsections. For zone-level analysis, there are two floors and each floor has five zones. They have similar patterns in regard to the sensitivity analysis. One zone from each floor (zone 102 and zone 204) was selected to demonstrate the sensitivity analysis.

5.2.1. System SA Analysis

The AHU power consumption was studied. Figure 17 illustrates the sensitivity index for cooling power. The cooling power is sensitive to the random errors of the SAT and OAT sensors, total errors of the SAT and OAT sensors, and bias errors of the SAT and OAT sensors. They have equal impacts on cooling power demands.

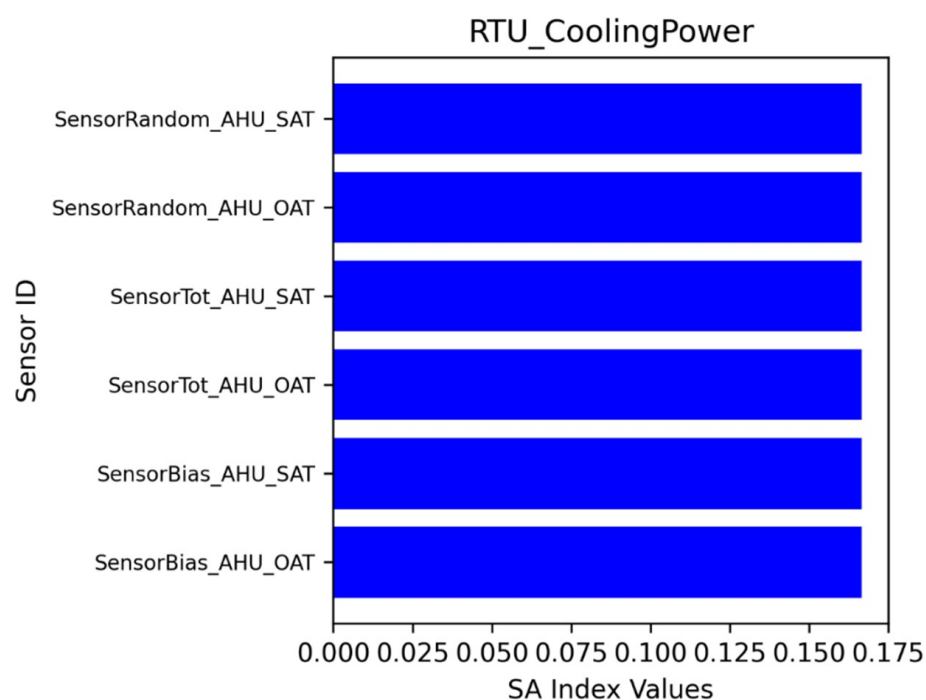


Figure 17. SA for RTU cooling power.

Figure 18 illustrates the sensitivity index for fan power demands. The sensor impacts are similar to the cooling power. Figure 19 illustrates the sensitivity index for main heating coil heating rates. The SAT and OAT sensors are the most dominant sensors.

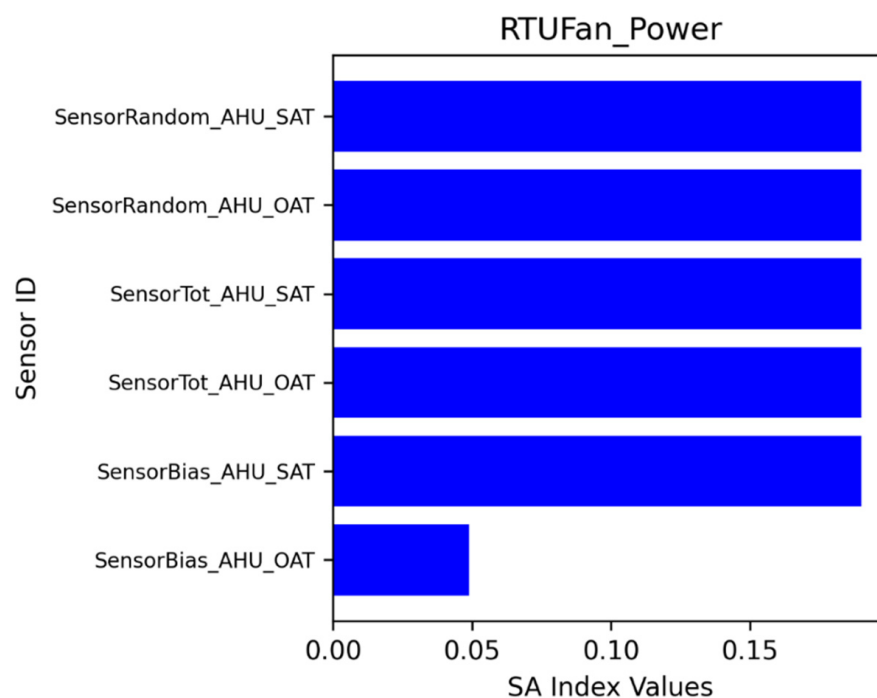


Figure 18. SA for RTU fan power.

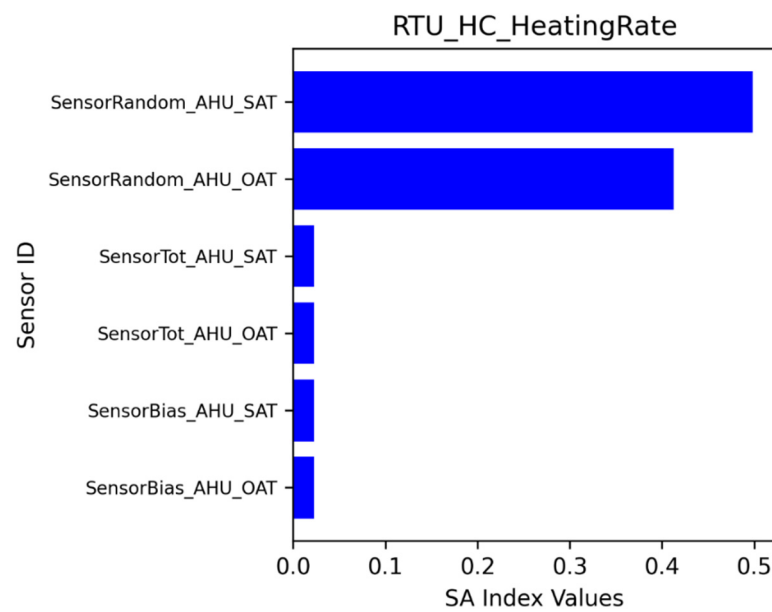


Figure 19. SA for RTU main heating coil heating rate.

5.2.2. Zone 204 SA Analysis

At the zone level, four energy consumption variables (zone temperature, zone sensible heating, zone sensible cooling, and reheat coil energy consumption) and one thermal comfort variable (zone-predicted percentage of dissatisfied occupants [PPD]) were selected. Figure 20 shows the ranking of the sensitivity index for zone air temperature. Overall, the system- and zone-level sensors affected the zone temperature. The sensor with the highest sensitivity index was the zone air temperature sensor with random error. The random errors were the most influential, followed by total errors and then bias errors. Figure 21 shows the ranking of the sensitivity index for zone sensible heating. The zone air temperature sensor with random error had the highest sensitivity index. Figure 22 shows the zone sensible cooling impacts from the sensors. Figure 23 shows the impacts on reheat coil energy. Figure 24 shows the sensitive index ranking for zone thermal comfort (PPD). Across zone 204 outputs, the random errors consistently had stronger impacts.

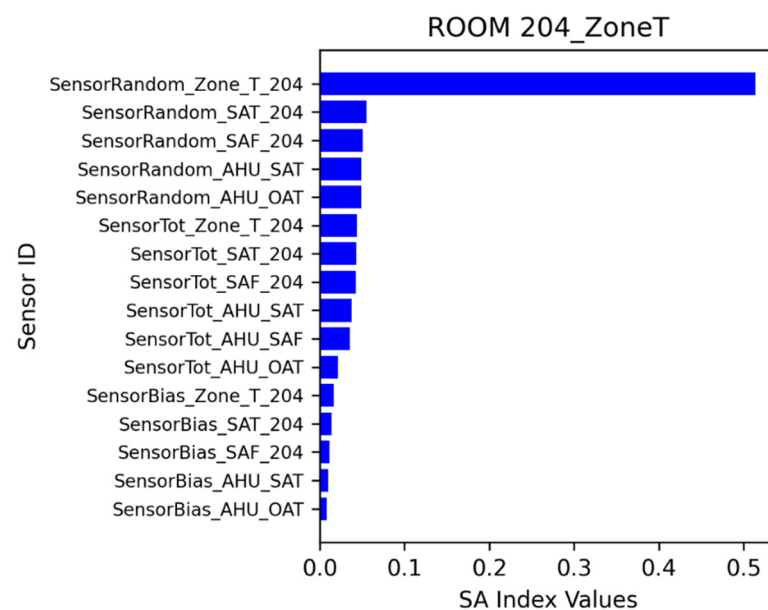


Figure 20. SA for zone 204 air temperature.

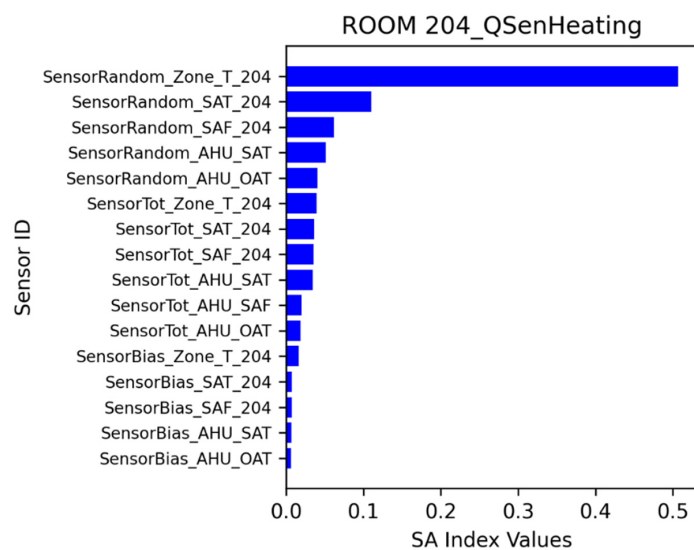


Figure 21. SA for zone 204 sensible heating.

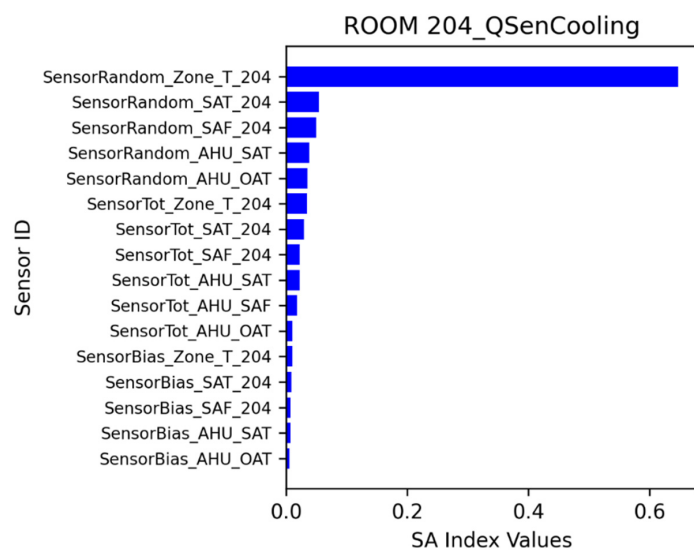


Figure 22. SA for zone 204 sensible cooling.

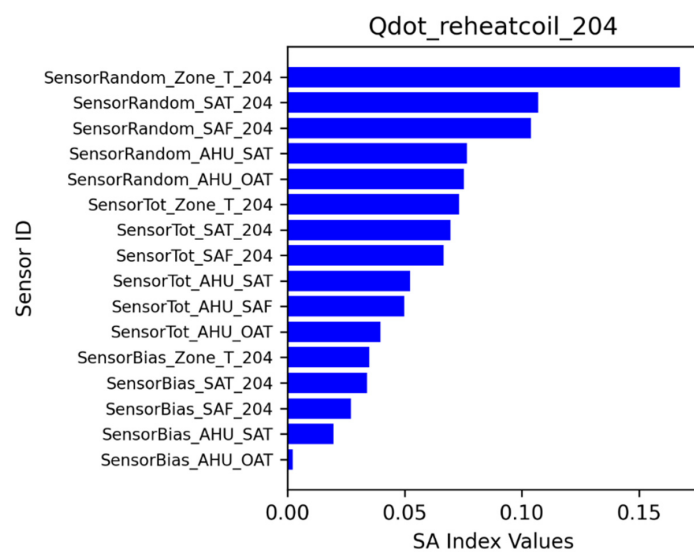


Figure 23. SA for zone 204 reheat coil energy.

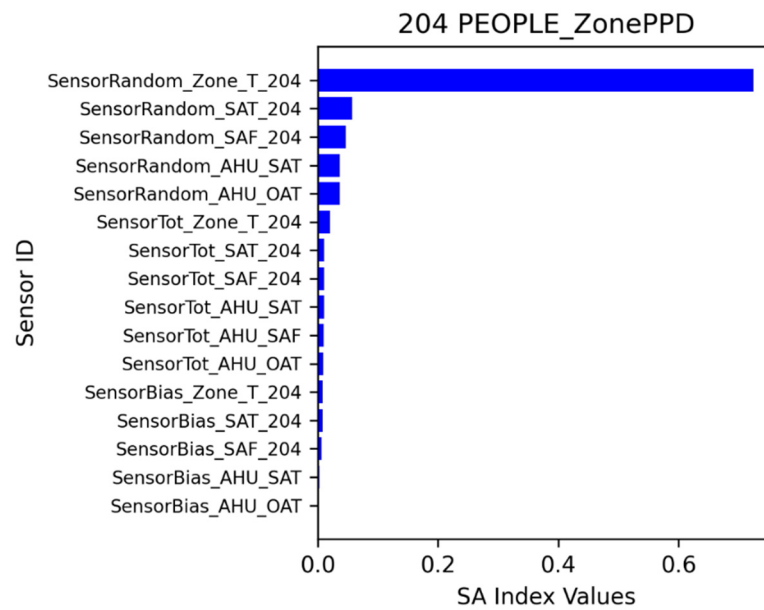


Figure 24. SA for zone 204 PPD.

5.2.3. Zone 102 SA Analysis

Sensitivity analysis for zone 102 was performed similarly to that of zone 204. The impacts of sensor errors on four energy consumption variables (zone temperature, zone sensible heating, zone sensible cooling, and reheat coil energy consumption) and one thermal comfort variable (zone PPD) were demonstrated. Figure 25 shows the ranking of the sensitivity index for zone 102 air temperature. The system-level sensors and zone-level sensors affected the zone temperature. The zone air temperature sensor with random error had the highest sensitivity index. Figure 26 shows the ranking of the sensitivity index for zone sensible heating. The zone air temperature sensor with random error had the highest sensitivity index. Figure 27 shows the zone sensible cooling impacts from the sensors. Figure 28 shows the impacts on reheat coil energy. Figure 29 shows the sensitivity index ranking for zone thermal comfort (PPD). Across zone 102 output variables, random errors consistently had stronger impacts.

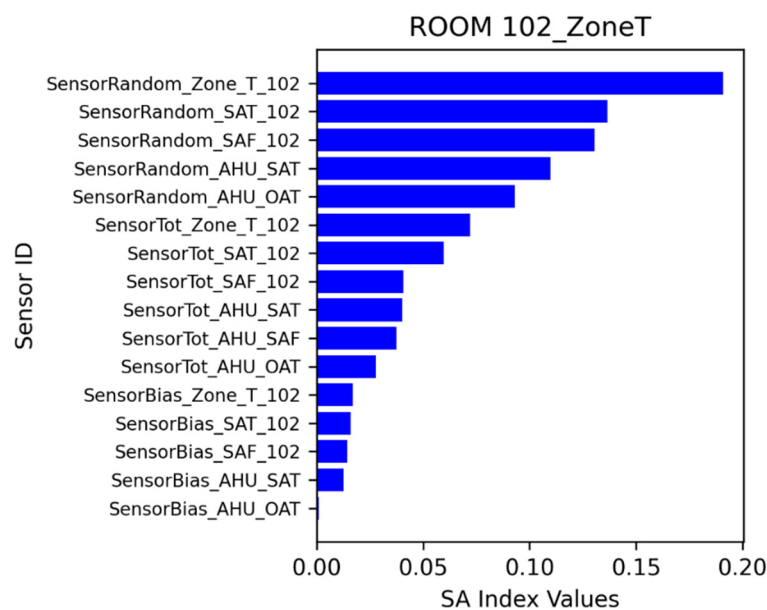


Figure 25. SA for zone 102 air temperature.

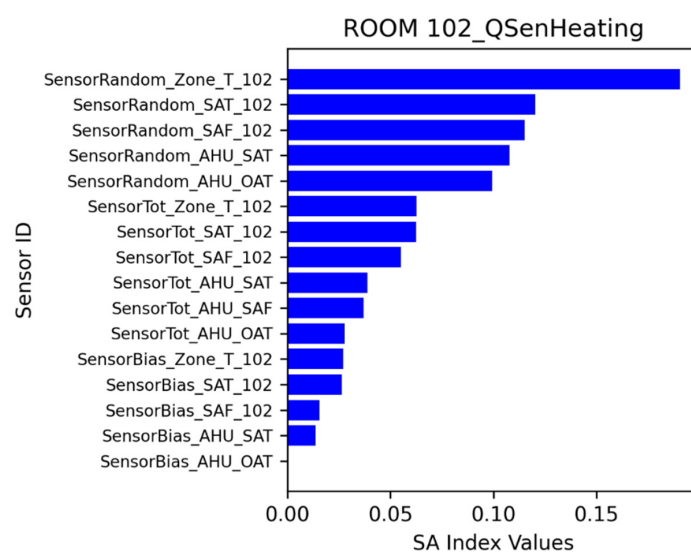


Figure 26. SA for zone 102 sensible heating energy.

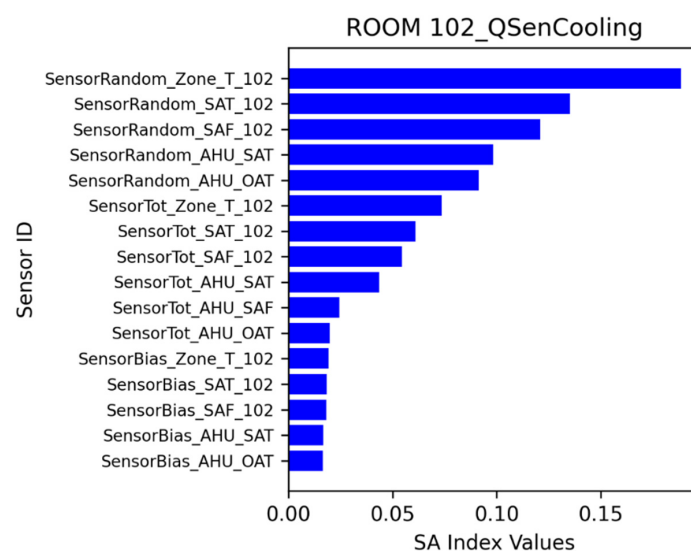


Figure 27. SA for zone 102 sensible cooling energy.

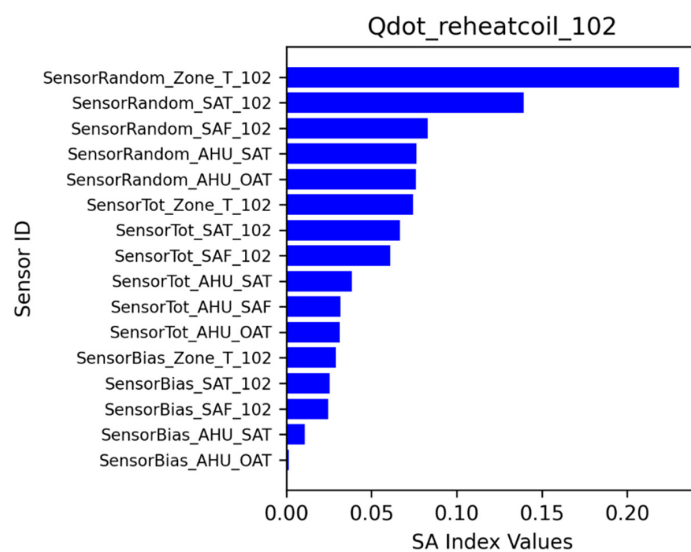


Figure 28. SA for zone 102 reheat coil energy.

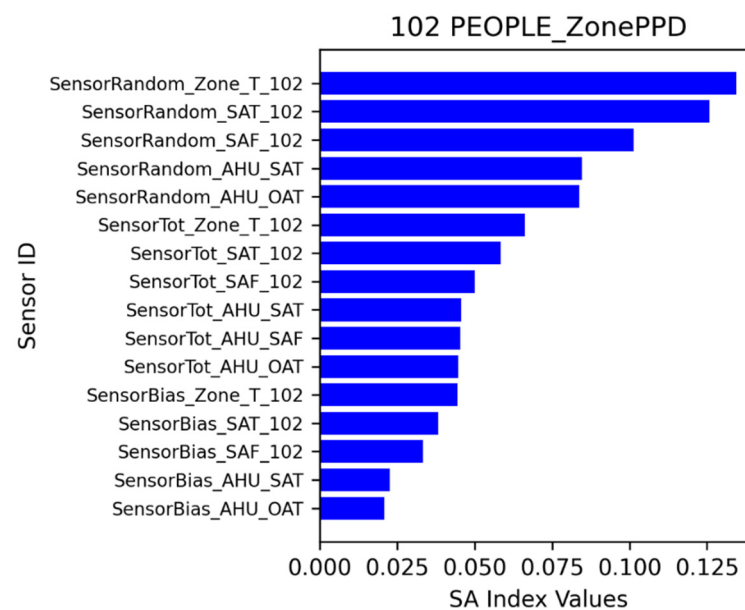


Figure 29. SA for zone 102 PPD.

6. Conclusions

This study investigated the incipient sensor impacts on the ASHRAE Guideline 36 control sequences through sensitivity and uncertainty analyses. The sensor errors had two components: bias error and precision (random) error. The sensor samplings were performed with normal distributions. Cloud simulations were conducted based on the sensor samplings and 3600 simulation cases. The results were collected to train surrogate models for sensitivity analysis.

The energy consumption was classified into system levels (power demands) and zone levels (zone air temperature, zone sensible heating, zone sensible cooling, and zone reheat coil energy). The thermal comfort (PPD) at the zone level was also investigated.

The uncertainty and sensitivity analyses were conducted with respect to sensor errors and energy/thermal comfort variables. The uncertainty analysis showed that the sensor errors and energy consumptions have a nonlinear relationship. The energy consumptions have wide distributions compared with the baseline model with sensor error uncertainties:

- The site energy differences could go -3.3% lower or 18.1% higher, compared with baseline;
- The heating energy differences could go -66.5% lower or 314.4% higher, compared with baseline;
- The cooling energy differences could go -11.5% lower or 65.0% higher, compared with baseline;
- The fan energy differences could go 0.15% lower or 6.9% higher, compared with baseline.

The sensitivity analysis was performed at both system and zone levels. At the system level, the random errors for SAT and OAT sensors had the most significant impacts. At the zone level, the random errors were the most influential, followed by total errors and then bias errors.

In the future, there are a few works worth exploring:

- Other sensitivity analysis methods will be used for comparative analysis;
- Other control strategies or HVAC systems will be used for more demonstrations.

This study clearly demonstrated the severe impacts of incipient sensor faults. The implications for research, policy, and study are: (1) calibrating sensors as recommended by the manufacturer. (2) if calibration is feasible, fault mitigations are recommended.

Author Contributions: Y.L.: Modeling development and simulations, Investigation, Data analysis, Writing—original draft, Writing—review & editing; P.I.: Supervision, Data analysis, Project management, Conceptualization, Investigation, Writing—review & editing, and Funding acquisition; S.L. (Seungjae Lee): Modeling development and simulation, Conceptualization, Investigation; Y.B.: Modeling development and simulation, Conceptualization, and Project management; Y.Y.: Modeling development and simulation, Writing—original draft, and Data analysis; S.L. (Sangkeun Lee): Modeling simulation. All authors have read and agreed to the published version of the manuscript.

Funding: This work was funded by field work proposal CEBT105 under DOE BTO activity nos. BT0302000 and BT0305000.

Acknowledgments: This material is based upon work supported by the US Department of Energy’s (DOE’s) Office of Science and Building Technologies Office (BTO). This research used resources of Oak Ridge National Laboratory’s Building Technologies Research and Integration, which is a DOE Office of Science User Facility. This work was funded by field work proposal CEBT105 under DOE BTO activity nos. BT0302000 and BT0305000. This manuscript has been authored by UT-Battelle LLC under contract DEAC05-00OR22725 with DOE. The US government retains and the publisher, by accepting the article for publication, acknowledges that the US government retains a nonexclusive, paid-up, irrevocable, worldwide license to publish or reproduce the published form of this manuscript, or allow others to do so, for US government purposes.

Conflicts of Interest: The authors declare that they have no known competing financial interests or personal relationships that could have appeared to influence the work reported in this paper.

References

1. Analysis & Projections—U.S. Energy Information Administration (EIA). Available online: <https://www.eia.gov/analysis/index.php> (accessed on 9 September 2022).
2. Liu, X.; Lu, S.; Hughes, P.; Cai, Z. A comparative study of the status of GSHP applications in the United States and China. *Renew. Sustain. Energy Rev.* **2015**, *48*, 558–570. [\[CrossRef\]](#)
3. Shen, B.; Ally, M.R. Energy and Exergy Analysis of Low-Global Warming Potential Refrigerants as Replacement for R410A in Two-Speed Heat Pumps for Cold Climates. *Energies* **2020**, *13*, 5666. [\[CrossRef\]](#)
4. Bae, Y.; Bhattacharya, S.; Cui, B.; Lee, S.; Li, Y.; Zhang, L.; Im, P.; Adetola, V.; Vrabie, D.; Leach, M.; et al. Sensor impacts on building and HVAC controls: A critical review for building energy performance. *Adv. Appl. Energy* **2021**, *4*, 100068. [\[CrossRef\]](#)
5. Li, Y.; O’Neill, Z. A critical review of fault modeling of HVAC systems in buildings. In Proceedings of the Building Simulation, Cambridge, UK, 11–12 September 2018; Springer: Berlin/Heidelberg, Germany, 2018; Volume 11, pp. 953–975.
6. Basarkar, M.; Pang, X.; Wang, L.; Haves, P.; Hong, T. *Modeling and Simulation of HVAC Faults in EnergyPlus*; Lawrence Berkeley National Lab. (LBNL): Berkeley, CA, USA, 2011.
7. Ni, K.; Ramanathan, N.; Chehade, M.N.H.; Balzano, L.; Nair, S.; Zahedi, S.; Kohler, E.; Pottier, G.; Hansen, M.; Srivastava, M. Sensor network data fault types. *ACM Trans. Sens. Netw. (TOSN)* **2009**, *5*, 1–29. [\[CrossRef\]](#)
8. Lu, X.; O’Neill, Z.; Li, Y.; Niu, F. A novel simulation-based framework for sensor error impact analysis in smart building systems: A case study for a demand-controlled ventilation system. *Appl. Energy* **2020**, *263*, 114638. [\[CrossRef\]](#)
9. Li, Y.; O’Neill, Z. An innovative fault impact analysis framework for enhancing building operations. *Energy Build.* **2019**, *199*, 311–331. [\[CrossRef\]](#)
10. O’Neill, Z.D.; Li, Y.; Cheng, H.C.; Zhou, X.; Taylor, S.T. Energy savings and ventilation performance from CO₂-based demand controlled ventilation: Simulation results from ASHRAE RP-1747 (ASHRAE RP-1747). *Sci. Technol. Built Environ.* **2020**, *26*, 257–281. [\[CrossRef\]](#)
11. Ye, Y.; Chen, Y.; Zhang, J.; Pang, Z.; O’Neill, Z.; Dong, B.; Cheng, H. Energy-saving potential evaluation for primary schools with occupant-centric controls. *Appl. Energy* **2021**, *293*, 116854. [\[CrossRef\]](#)
12. Pang, Z.; Chen, Y.; Zhang, J.; O’Neill, Z.; Cheng, H.; Dong, B. Nationwide HVAC energy-saving potential quantification for office buildings with occupant-centric controls in various climates. *Appl. Energy* **2020**, *279*, 115727. [\[CrossRef\]](#)
13. Maasoumy, M.; Razmara, M.; Shahbakhti, M.; Vincentelli, A. Handling model uncertainty in model predictive control for energy efficient buildings. *Energy Build.* **2014**, *77*, 377–392. [\[CrossRef\]](#)
14. Bengae, S.; Adetola, V.; Kang, K.; Liba, M.J.; Vrabie, D.; Bitmead, R.; Narayanan, S. Parameter estimation of a building system model and impact of estimation error on closed-loop performance. In Proceedings of the 2011 50th IEEE Conference on Decision and Control and European Control Conference, Orlando, FL, USA, 12–15 December 2011; pp. 5137–5143.
15. Chen, J.; Zhang, L.; Li, Y.; Shi, Y.; Gao, X.; Hu, Y. A review of computing-based automated fault detection and diagnosis of heating, ventilation and air conditioning systems. *Renew. Sustain. Energy Rev.* **2022**, *161*, 112395. [\[CrossRef\]](#)
16. Yoon, S.; Yu, Y.; Wang, J.; Wang, P. Impacts of HVACR temperature sensor offsets on building energy performance and occupant thermal comfort. In Proceedings of the Building Simulation, Rome, Italy, 2–4 September 2019; Springer: Berlin/Heidelberg, Germany, 2019; Volume 12, pp. 259–271.

17. Kim, J.; Frank, S.; Braun, J.E.; Goldwasser, D. Representing small commercial building faults in energypplus, Part I: Model development. *Buildings* **2019**, *9*, 233. [CrossRef]
18. Kim, J.; Frank, S.; Im, P.; Braun, J.E.; Goldwasser, D.; Leach, M. Representing small commercial building faults in EnergyPlus, part II: Model validation. *Buildings* **2019**, *9*, 239. [CrossRef]
19. Zhao, Y.; Li, T.; Zhang, X.; Zhang, C. Artificial intelligence-based fault detection and diagnosis methods for building energy systems: Advantages, challenges and the future. *Renew. Sustain. Energy Rev.* **2019**, *109*, 85–101. [CrossRef]
20. Wang, P.; Li, J.; Yoon, S.; Zhao, T.; Yu, Y. The detection and correction of various faulty sensors in a photovoltaic thermal heat pump system. *Appl. Therm. Eng.* **2020**, *175*, 115347. [CrossRef]
21. Gunes, V.; Peter, S.; Givargis, T. Improving energy efficiency and thermal comfort of smart buildings with HVAC systems in the presence of sensor faults. In Proceedings of the 2015 IEEE 17th International Conference on High Performance Computing and Communications, New York, NY, USA, 24–26 August 2015; IEEE: Piscataway, NJ, USA, 2015; pp. 945–950.
22. Zhang, L.; Leach, M.; Bae, Y.; Cui, B.; Bhattacharya, S.; Lee, S.; Im, P.; Adetola, V.; Vrabie, D.; Kuruganti, T. Sensor impact evaluation and verification for fault detection and diagnostics in building energy systems: A review. *Adv. Appl. Energy* **2021**, *3*, 100055. [CrossRef]
23. Cheung, H.; Braun, J.E. Empirical modeling of the impacts of faults on water-cooled chiller power consumption for use in building simulation programs. *Appl. Therm. Eng.* **2016**, *99*, 756–764. [CrossRef]
24. ASHRAE Guideline 36-2018: High-Performance Sequences of Operation for HVAC Systems 2022. Available online: <https://www.techstreet.com/ashrae/standards/guideline-36-2018-high-performance-sequences-of-operation-for-hvac-systems> (accessed on 9 September 2022).
25. Im, P.; Joe, J.; Bae, Y.; New, J.R. Empirical validation of building energy modeling for multi-zones commercial buildings in cooling season. *Appl. Energy* **2020**, *261*, 114374. [CrossRef]
26. Taylor, S. Resetting setpoints using trim & respond logic. *Ashrae J.* **2015**, *11*, 52–57.
27. Hochreiter, S.; Schmidhuber, J. Long short-term memory. *Neural Comput.* **1997**, *9*, 1735–1780. [CrossRef]
28. Tian, W. A review of sensitivity analysis methods in building energy analysis. *Renew. Sustain. Energy Rev.* **2013**, *20*, 411–419. [CrossRef]
29. Pang, Z.; O'Neill, Z.; Li, Y.; Niu, F. The role of sensitivity analysis in the building performance analysis: A critical review. *Energy Build.* **2020**, *209*, 109659. [CrossRef]

Disclaimer/Publisher's Note: The statements, opinions and data contained in all publications are solely those of the individual author(s) and contributor(s) and not of MDPI and/or the editor(s). MDPI and/or the editor(s) disclaim responsibility for any injury to people or property resulting from any ideas, methods, instructions or products referred to in the content.